Bonding and hardness in nonhydrogenated carbon films with moderate sp^3 content

R. Gago,[a] I. Jiménez, and J. M. Albella
Instituto de Ciencia de Materiales de Madrid (CSIC), 28049 Madrid, Spain

A. Climent-Font
Departmento de Física Aplicada (C-XII), Universidad Autónoma de Madrid. 28049 Madrid, Spain

D. Cáceres and I. Vergara
Departmento de Física Aplicada, Universidad Carlos III de Madrid, 28911 Leganés, Spain

J. C. Banks and B. L. Doyle
Sandia National Laboratories, Radiation Solid Interactions and Processing. Albuquerque, New Mexico 87185-1056

L. J. Terminello
Lawrence Livermore National Laboratory, Livermore, California 94550

(Received 29 October 1999; accepted for publication 6 March 2000)

Amorphous carbon films with an sp^3 content up to 25% and a negligible amount of hydrogen have been grown by evaporation of graphite with concurrent Ar^+ ion bombardment. The sp^3 content is maximized for Ar^+ energies between 200 and 300 eV following a subplantation mechanism. Higher ion energies deteriorate the film due to sputtering and heating processes. The hardness of the films increases in the optimal assisting range from 8 to 18 GPa, and is explained by crosslinking of graphitic planes through sp^3 connecting sites. © *2000 American Institute of Physics.* [S0021-8979(00)08911-8]

I. INTRODUCTION

Amorphous carbon (*a*-C) has been the object of intense research in recent decades because of its unique properties and applications. The properties of this material depend strongly on the presence of hydrogen in the structure and the sp^3 content.[1] The incorporation of hydrogen increases the stability by providing stress relief but decreases the mechanical performance of the films, which become more polymeric.[2] The sp^3 hybridization give the material diamond-like properties such as high hardness, infrared transparency, and chemical inertness.[3] This is basis of a classic classification of carbon films, which is summarized in the well-known triangle of compositions with sp^3 carbon, sp^2 carbon, and hydrogen located at the vertex.[4]

However, a new scenario appeared with the discovery of fullerenes[5] and carbon nanotubes,[6] and the realization that films composed of sp^2 carbon with curved basal planes resembling fullerene structures can exhibit high hardness and elasticity.[7] Nowadays, there is a renewed interest in graphitic carbon films with good mechanical properties such as hardness up to 40 GPa and free from internal stress. These properties are explained by the curvature and cross linking of basal planes, due to the presence of pentagonal and heptagonal ring defects[8] or sp^3 line defects.[9]

Energetically, the sp^2 structure is the most favorable and the one attained unless hyperthermal carbon atoms are used. When carbon atoms with ~100 eV reach the surface, the number of sp^3 bonds is increased due to subplantation effects.[10,11] The impinging carbon atoms get their high energy either by direct acceleration (ion beam deposition) or, indirectly by knock-on collisions with assistant inert ions [ion beam assisted deposition (IBAD)]. In our case, carbon is thermally evaporated and the assistance is performed with a beam of Ar^+ ions.

In this work we report the hardness, elasticity, and bonding structure of amorphous carbon films with a moderate sp^3 content of ~30%. The aim of this work is twofold. First, we want to explore the possibilities of a simple technique like IBAD for the growth of hard carbon films, in comparison with the more sophisticated ion filtered methods. Second, we search for information on the bonding structure of amorphous carbon using short-range order techniques like x-ray near edge absorption spectroscopy (XANES) in combination with Raman spectroscopy.

II. EXPERIMENT

A. Film deposition

Amorphous carbon films were grown in a high vacuum chamber with a base pressure of 2×10^{-7} mbar on *p*-type (100) oriented Si substrates. The system is equipped with a 5 kW electron-gun evaporator and a 3 cm diam Kauffman ion gun for assistance. The Si wafers were chemically cleaned in an ultrasonic bath prior entering the vacuum chamber. Further cleaning was performed with an Ar^+ beam of 300 V before deposition. The carbon beam was obtained by evaporating graphite lumps at a rate of 2 Å/s. The evaporation was assisted with a concurrent Ar^+ ion beam. The ion assisting

[a]Author to whom correspondence should be addressed; electronic mail: rgf@icmm.csic.es

current was fixed at 10 mA (yielding an ion to carbon ratio, I/A, of 5) and the acceleration voltage was varied between 0 and 800 V. The I/A value was chosen in the range where ion induced damage is low.[12] The deposition time was 15 min for all the samples and the substrates were held at a temperature below 100 °C.

B. Film characterization

The film thickness was measured with a Dektak 3030 profiling system. Considering the apparatus resolution and the film roughness, the thickness was determined with a resolution of ~15 nm. For the typical thickness of our films, between 100 and 300 nm, the accuracy in the measure ranges between 5% and 10%.

Rutherford backscattering spectrometry (RBS) and elastic recoil detection analysis (ERDA) techniques were used to determine the composition and areal density of the films. The experiments were carried out with the tandem accelerator facility at Sandia National Laboratories. ORTEC commercial detectors with a depletion depth of 300 μm and an active area of 300 mm^2 were used. The energy resolution of the detector was calibrated with a standard, resulting in 19 keV per channel for α particles. The product of the dose and solid angle was 2.42×10^{11} and 6.8×10^{10} particles sr for the RBS and ERDA experiments, respectively. RBS was performed with 3.73 MeV ^{4}He and 164° scattering angle. At this energy, the scattering cross section for the carbon is non-Rutherford, with a signal enhanced by about seven times the Rutherford value.[13,14] ERDA measurements were performed with 26 MeV ^{28}Si ions and a range foil of Mylar 12 μm thick. The incident angle in the scattering geometry was 75° and the exiting angle 75°, leading to a scattering angle of 30°. With this configuration carbon and hydrogen are well detected giving nonoverlapping signals. The oxygen present in the film is also detected, although the signal partially appears in the low energy side of the spectrum. The quantification of the RBS and ERDA spectra was done with the computer code SIMNRA.[15] This code allows the simulation of the experimental spectra using Rutherford scattering cross section values, as well as non-Rutherford values, using tabulated data existing in the literature.

Detailed information on the bonding structure was obtained with XANES. This technique is sensitive to the bonding environment and works well in amorphous and nanocrystalline systems. It is especially interesting for carbon-based materials since it yields very different spectral line shapes for graphite and diamond with similar cross sections.[16,17] The XANES experiments were performed at the beamline 8.2 of the Stanford Synchrotron Radiation Laboratory. The data were collected in the total yield mode by recording the sample current to ground and normalized to the signal coming from a gold-covered grid located upstream in the x-ray path. The angle between the sample normal and the incident light was near 55° to avoid preferential bond orientation effects, except when performing angle dependent studies.

Visible Raman spectroscopy was used to study the microstructure of the films, since the technique is very sensitive to the graphitic grain size and gives information about the long-range order. The spectra were obtained with a DILOR $x-y$ microRaman system using the 514 nm line of an Ar laser. In visible Raman spectroscopy of carbon films the efficiency for sp^2 bonds is about 50 times that of sp^3.[18] This drawback makes it difficult to quantify the sp^2/sp^3 content, although it provides additional structural information.[19]

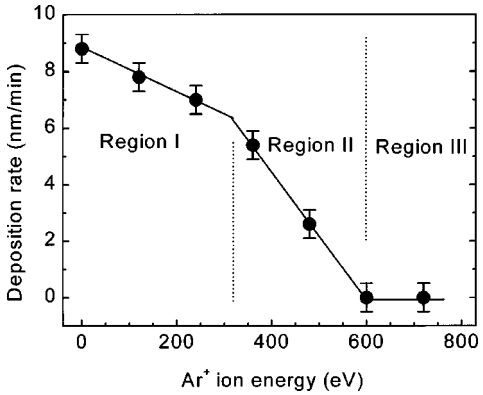

FIG. 1. Deposition rate for a set of films grown at different ion assisting energies. Three different regimes are found regarding the ion–carbon atoms interactions.

Nanoindentation experiments were made using a Nano Indenter® II (Nano Instruments, Inc). The load-displacement data obtained were analyzed using the method of Oliver and Pharr[20] to determine the hardness as a function of the displacement of the indenter. In each indentation experiment, the indenter was loaded and unloaded three times, at a constant rate of 10% of the maximum depth per second. Each unloading was terminated at 10% of the peak load to ensure that the contact was maintained between the specimen and the indenter. Three hold periods of 10 s were inserted at the maximum depths and another hold period of 100 s was at the minimum of the final unloading. During this last hold period the displacement of the indenter was carefully monitored to establish the rate of thermal drift in the machine for subsequent correction of the data. Hardness results correspond to a penetration depth ~10% of the film thickness to avoid the influence of the substrate.[21,22] Each indentation experiment was performed ten times in each sample and the mean value of hardness was taken as the result of the measure.

III. RESULTS

A. Growth rate, composition, and density

The thickness of the films has been determined by profilometry. The measurement was performed at four different points within each sample, revealing a good homogeneity of the films. Figure 1 displays the growth rate, i.e., thickness over deposition time, for the set of samples grown under different assisting voltages. It is clear that increasing the voltage implies a reduction in the deposition rate. However, the decay is not constant for the whole voltage range and different regions are observed.

Since the flux of carbon atoms reaching the substrate is kept constant for the whole set of samples, the decrease in the growth rate is explained by either a densification of the film, or a resputtering of the condensed carbon atoms. The

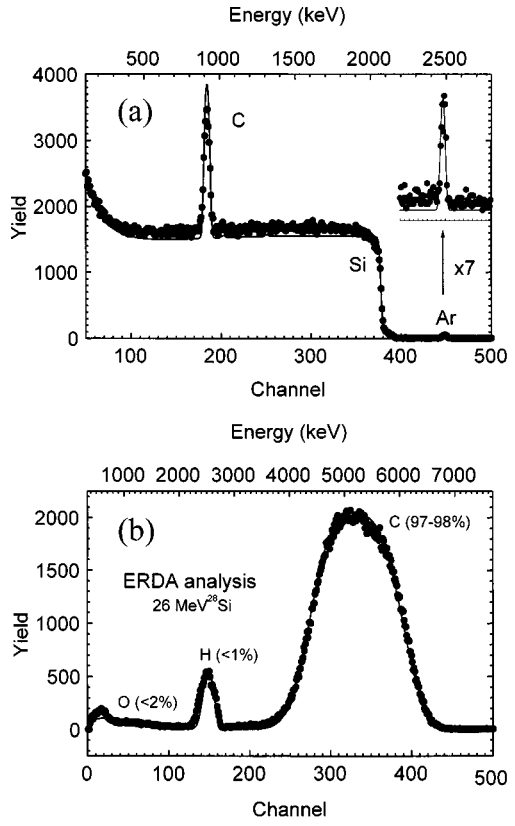

FIG. 2. RBS (a) and ERDA (b) spectrum for the sample grown with assistance of 120 eVAr^+ ions. The experimental spectra are shown with dots and the simulation with continuous line.

densification is induced by momentum transfer of the Ar^+ ions to the impinging carbon atoms, producing dense sp^3 configurations and annealing out the vacancies present in evaporated carbon films.[23] Resputtering of the carbon atoms is produced when the displacement energy of the deposited atoms is overcome during bombardment.[24] The densification process is dominant in region I. The fast decay in region II indicates a dominant sputtering regime in this voltage range, until no films are grown in region III.

The techniques RBS, detecting C, N, O, and Ar, and ERDA, detecting C, H, and O, give complementary information on the film composition. The use of both ion beam techniques (RBS and ERDA) provides a better accuracy in the analysis, since the same sample composition has been assumed in the simulation of both spectra. Figure 2 shows the RBS (panel a) and ERDA (panel b) spectra of the sample grown with an assistance voltage of 120 V. The experimental curve is represented with dots and the simulated spectrum with a continuous line. The enhancement of the C signal in the RBS spectrum due to the non-Rutherford cross section value is evident.

Table I contains the compositional results from the ion beam analysis. The films are mainly composed of carbon with a small amount of argon, oxygen, and hydrogen. The hydrogen content in the films is very small and comes mainly from surface hydrocarbon contamination. This assumption has been corroborated by simulating a thin layer of contaminant in the surface of the film. Also, recent time of flight ERDA measurements on similar samples, a technique that provides a composition depth profile, indicate that hydrogen appears in the surface region.[25] The argon content that is incorporated into the film as a result of the ion bombardment is limited to 3 at. %. Finally, the oxygen content (below 2 at. %) corresponds to surface contamination, as was verified by the decrease in the O(1*s*) XANES signal after heating the sample over 250 °C.

TABLE I. Composition results from the ion beam analysis of the carbon samples shown in Fig. 1.

Assistance voltage (V)	at. % C	at. % Ar	at. % O	at. % H
0	98	0	1	1
120	96	1	2	1
240	93	3	2	2
360	95	3	1	1
480	95	2	1	2

The film density was determined by dividing the areal density provided by the ion beam analysis (RBS and ERDA) over the thickness of the films as measured by profilometry. In our case, we have only taken into account the density of carbon atoms to avoid the fact that the higher mass of Ar atoms massk the calculated values. The resulting values are illustrated in Fig. 3. The uncertainty of the density values ranges between 5% and 10%, mainly affected by the accuracy of the thickness measurements. The uncertainty is larger for the thinner films and, hence, the density of the films grown with voltages over 400 V is not considered. Note that the density of the carbon film evaporated without assistance is lower than the density of crystalline graphite (2.2 g/cm^{-3}), due to the presence of microvoids in the amorphous graphitic network.[26] The data in Fig. 3 confirm the densification of the carbon films with the ion assistance in region I of Fig. 1.

B. X-ray absorption near edge spectroscopy

XANES has been used to quantify the sp^3 content and obtain information on the bonding structure. The measurements were repeated in several points of each sample with identical results, confirming the homogeneity of the films. Figure 4 shows photoabsorption spectra at the C(1*s*) edge, normalized to the same height, for the whole set of films considered in this study, together with highly oriented pyroli-

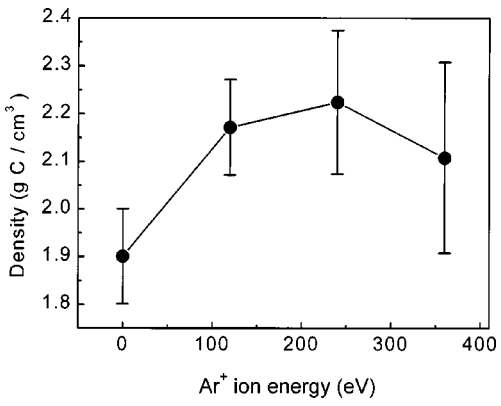

FIG. 3. Density of the carbon films as a function of the assisting ion energy.

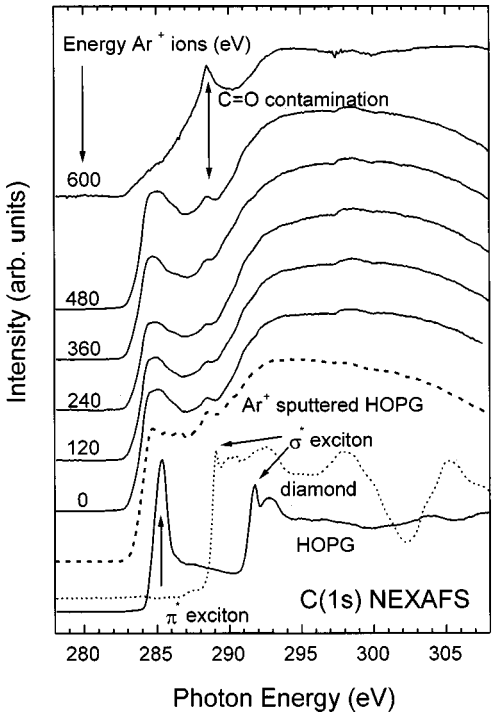

FIG. 4. XANES C(1*s*) spectra of amorphous carbon films grown with different Ar^+ ion assistance energies. Highly oriented pyrolitic graphite (HOPG), sputtered HOPG, and diamond reference spectra are also shown.

tic graphite (HOPG) and crystalline diamond references, and a reference spectrum from HOPG sputtered with 1 keV Ar^+ ions to produce an amorphous carbon film with 100% sp^2. The graphite spectrum shows an absorption threshold of transition to π^* states at 284 eV and a second threshold of transitions to σ^* states at 291 eV. Diamond lacks π^* states and hence shows a single absorption edge at 289 eV.

The overall shape of the amorphous carbon spectra is similar except for the sample grown with the assistance of 600 eV ions. As shown in Fig. 1, under those conditions no film is grown due to dominant sputtering processes, and the XANES signal is dominated by the C═O surface contamination on the silicon substrate.[27] The films grown with 0–480 V ion assistance show a π^* peak characteristic of sp^2 bonded carbon, although much broader than the graphite reference. The broad π^* feature in the *a*-C films presents structure, indicating the presence of several bonding environments related to defects in the graphitic coordination and bonding between sp^2 and sp^3 hybridized C atoms. The σ^* region starts at 289 eV, representing states from sp^3 hybrids, and merges with the σ^* states from sp^2 hybrids that appear beyond 291 eV. The spectra do not show separated σ^* absorption edges related to segregated sp^2 and sp^3 phases and indicates that mixing of sp^2 and sp^3 carbon occurs at the atomic level. These are the features commonly found in amorphous diamond-like carbon.[28,29]

The quantification of the sp^2/sp^3 content in the films is derived from the relative intensity ratio of π^*/σ^* states, as used in EELS measurements.[30] This method considers the decrease of the π^* intensity as being due to the increase of the sp^3 content, and is accepted as the most reliable way of quantifying the sp^3 content in *a*-C films. The use of XANES has the advantage over EELS of a better resolution and, hence, there is no overlapping of π and σ states. For computing purposes, the area between 282 and 287 eV was assigned to π^* states and the area between 294 and 301 eV to σ^* states. The intensity ratios were compared with the spectrum from the Ar^+ sputtered HOPG, whose sp^2 content is 100%. One cannot use as reference the HOPG spectrum because the π^* peak has an excitonic origin and its intensity depends on the microstructure, which affects electron localization.[31] Actually, the relative π^* intensity from the Ar^+ sputtered HOPG is only 80% of the intensity from HOPG. The π^* intensity ratio and the corresponding sp^2 content are displayed in Fig. 5 for the whole set of films. The analysis reveals an optimal range between 200 and 300 V for the promotion of sp^3 atoms.

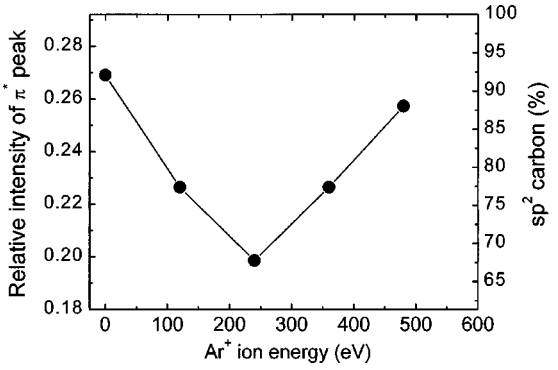

FIG. 5. Relative intensity of the π^* features in the XANES spectra of Fig. 4 and the corresponding sp^2 content.

Finally, an angle dependent XANES study (not shown) has been performed on several samples to determine whether preferential orientation of sp^2 phases occurs in the films, as has been observed in other ion assisted growth processes.[32] The present films are completely isotropic, without any preferential orientation.

C. Raman spectroscopy

Figure 6 shows the first order Raman spectra, normalized to the same height, for the set of samples previously considered. The samples grown with 600 and 720 V do not yield appreciable signal. The Raman spectra consist of two broadbands. The first band, commonly labeled as *G* (graphite), is located around 1580 cm^{-1} and arises from in-plane vibrations of the graphite-like rings. This band is related to the sharp and intense Raman peak at 1580 cm^{-1} in crystalline graphite. This peak broadens and shifts to lower values with decreasing crystallite size. The second band, labeled *D* (disorder), is located around 1360 cm^{-1} and only appears when small crystallites are formed. It corresponds to phonons with nonzero wave vector in a graphitic network, which are selection rule prohibited in a perfect crystal but become visible in nanodomains due to uncertainty in the wave vector.

Raman spectroscopy has been widely used to characterize amorphous carbon, despite the indirect information obtained. Raman cannot guarantee the presence of sp^3 bonding unless the 1330 cm^{-1} peak of crystalline diamond is ob-

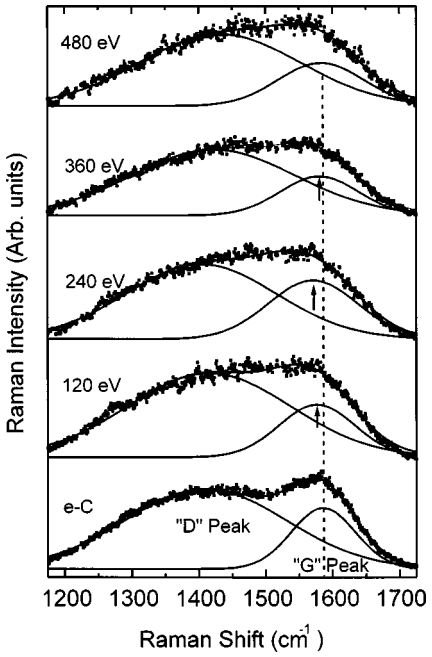

FIG. 6. Raman spectra of the films considered in Fig. 1. The spectra have been fitted with two Gaussian distributions labeled as G (graphite) and D (disordered).

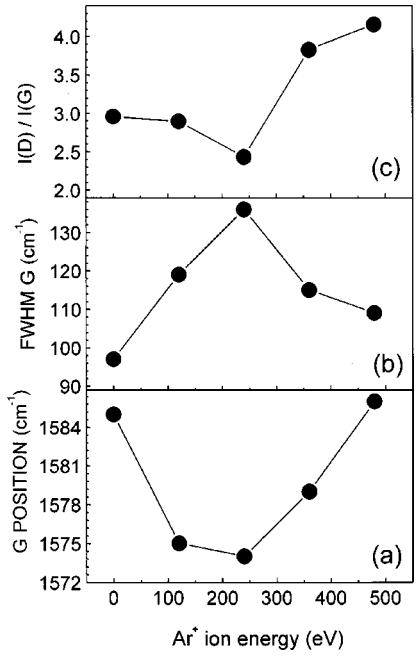

FIG. 7. (a) Position of the Raman G peak, (b) full width at half maximum (FWHM) for the G peak, and (c) intensity ratio of the ''disordered'' to ''graphite'' Raman peaks as a function of the assisting ion energy.

served, but provides interesting information on the microstructure of graphitic domains based on the following. The downshifting of the *G* peak is due to the graphitic bond angle disorder.[33] The width of the *G* peak increases with decreasing graphitic domain size,[34,35] ranging its full width at half maximum (FWHM) from 14 cm^{-1} in crystalline graphite to ~100–200 cm^{-1} in amorphous films. The intensity ratio $I(D)/I(G)$ of the *D* to *G* peaks increases inversely proportional to the grain diameter in the 300–2.5 nm range[36] and decreases directly proportional for smaller domain sizes.[37]

To determine the position, width and height of the *G* and *D* peaks one needs to perform a curve fitting analysis. Different criteria and curve fitting methods of the Raman spectra from amorphous carbon appear in the literature, although none of them is totally accepted. The most simple and common procedure considers two Gaussian distributions related to the *G* and *D* components, centered at ~1580 and ~1350 cm^{-1},[19,38] and it is the one used here.

The fitting parameters of the Raman spectra are shown in Fig. 7. The position of the *G* peak [Fig. 7(a)] shows a minimum around 200–300 V corresponding to a maximum bond-angle disorder. The similar behavior of the sp^3 content in Fig. 5 indicates a correlation between both parameters. The values of the FWHM [Fig. 7(b)] are consistent with the lack of long range order in the graphitic phases of our films, with a maximum disorder for the highest sp^3 content. The values of $I(D)/I(G)$ [Fig. 7(c)] also indicate a minimum size of the graphitic grains for the maximum sp^3 content.

D. Hardness

Figure 8 displays the hardness as a function of the indenter displacement for the films grown with 0, 120, and 240 V. The results for the sample grown voltages beyond 240 V are not reliable since the films are too thin and the hardness measurements are affected by the substrate. Figure 8 clearly indicates a hardness increase with the ion assistance from 8 to 18 GPa for the optimal range discussed previously. The elastic modulus follows well the relation $H/E \sim 0.1$ found in diamond that indicates good elastic behavior.

IV. DISCUSSION

Following the motivation of our study, the IBAD growth technique and the bonding structure of the amorphous carbon films are discussed as follows.

A. IBAD growth method

The IBAD method has been applied to the growth of amorphous carbon films, resulting in moderate sp^3 contents. During the growth of carbon films the resulting high stress induces a transformation of sp^2 carbon to sp^3.[26] The promotion of sp^3 is attained when carbon atoms impinge the sub-

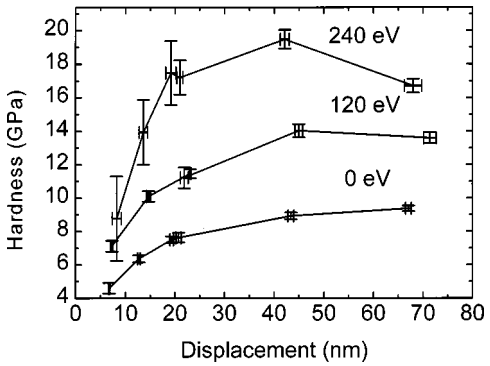

FIG. 8. Hardness of the carbon films as a function of the indentation depth, for different assisting ion energies.

strate with an optimal value around 100 eV, as described by a subplantation model.[39] In this context, some particularities of the IBAD technique used here are worth discussing. The carbon atoms are accelerated through momentum transfer in Ar^+–C collisions. In the collision, the energy transfer depends on the ion energy, ion to carbon atom ratio, assisting ion mass M, atom mass m, and scattering angle ϕ. The low sp^3 content of ~30% achieved in our deposition method seems a limitation of the assistance technique considering two major issues. First, only a small fraction of the carbon atoms reaching the substrate penetrate the subsurface layers with an optimal energy ~100 eV, necessary for sp^3 promotion. Second, the Ar^+ bombardment produces damage in the growing film. A higher ion/atom ratio would increase the number of ion–atom collisions and, hence, the energy transfer, but will result in a higher damage.

The maximum energy transfer is derived from the kinetic factor γ of the collision, which is 0.36 in our case. This value explains our maximum sp^3 content for acceleration voltages of 200–300 V, which correspond to incident carbon atoms with energy of 78–108 eV, close to the optimal 100 eV found in direct ion beam deposition. Similar results have been reported by other IBAD systems.[40,41] The ion energy range capable of promoting sp^3 sites when IBAD techniques are used is narrower than that found for direct ion beam deposition. With the latter technique, large sp^3 contents are found for ion energies as high as 1 keV, provided the substrate is accurately kept at room temperature,[42] this being consistent with the subplantation model. The fast decrease of the sp^3 content for high ion energies in IBAD is due to the damage induced by the Ar^+ bombardment and thermal annealing due to ion stopping.[43]

B. Microstructure and bonding structure

In the optimal energy range of ion assistance, the XANES results indicate a decrease of the density of π^* states that is attributed to formation of sp^3 hybrids, and the Raman results show a change of line shape corresponding to a decrease of the graphitic domain size. Both results are consistent with the formation of a network of graphitic planes interconnected through sp^3 sites. The smaller the graphitic domain, the larger the fraction of sp^3 connecting sites. The increase of the sp^3 content affects linearly the film density as is shown in Fig. 9. This linear relationship has been reported by other authors for amorphous carbon films grown by different deposition methods and is characteristic of diamondlike carbon.[40,44]

Regarding the types of bonding present in the films, we anticipated in Sec. III B that there is mixing of sp^2 and sp^3 sites at the atomic level, without segregated sp^3 phases. The bonding between sp^2 and sp^3 sites is of σ type. The π bonding within the graphitic domains reflects on the XANES π^* density of states, which is shown in detail in the lower panel (a) of Fig. 10. The HOPG and Ar^+ sputtered references are also displayed. Note how the π^* states from defective graphitic environments in sputtered HOPG extend ~1 eV below the π^* resonance in HOPG. The a-C spectra were normalized to the minimum intensity at 287 eV, in the valley between the π^* and the σ^* states. Small differences are found in the spectral line shape of a-C that are highlighted in the top panel (b) of Fig. 10 by subtracting from each spectrum the signal from the evaporated film without assistance.

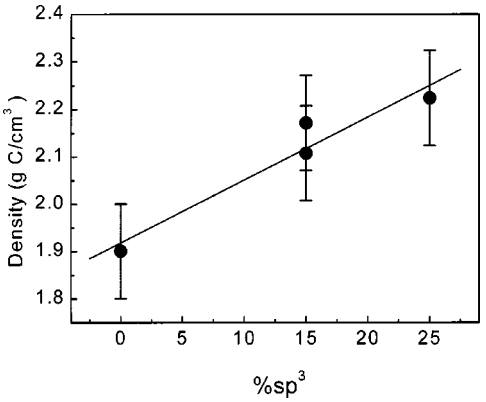

FIG. 9. Density of the carbon films as a function of the sp^3 content.

For bombardment with ions of energy below 240 eV, i.e., the region where formation of new sp^3 sites takes place, there is a decrease of the density of π^* states in the 284.5–287 eV region, and a slight increase of defect states at ~284

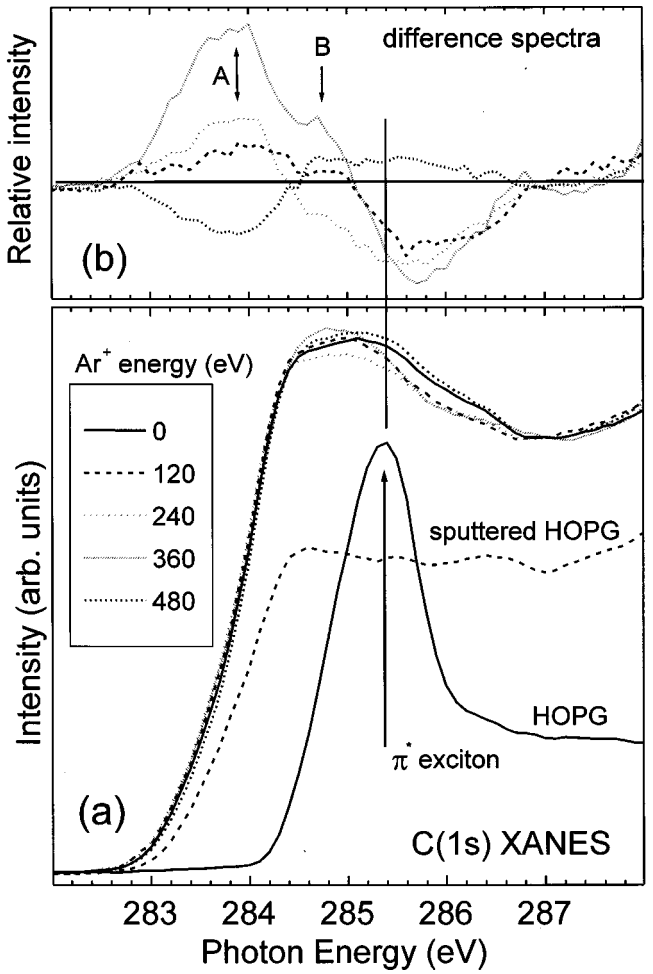

FIG. 10. Bottom panel (a) detailed view of the π^* region of the XANES C(1s) spectra for the amorphous carbon films of Fig. 4. Top panel (b) difference spectra obtained by subtracting from each spectrum the signal from the evaporated film without assistance.

eV, labeled *A* states. For ion energies beyond the optimal 240 eV value, the amount of defect states *A* increases significantly, and new defect states *B* at ~285 eV appear. This is explained by the damage created by the increasing ion bombardment that transforms sp^3 sites into sp^2 sites, with an enlargement of the graphitic domains. Finally, at an ion energy of 480 eV the initial line shape is almost recovered, presumably due to the annealing induced by the ion stopping.

The proposed bonding scheme permits us to explain the observed mechanical properties of the films, with a significant increase of the hardness from 8 to 18 GPa, for a small change in the sp^3 content. The crosslinking of graphitic planes through tetragonal sp^3 sites would confer on the carbon network a three-dimensional structure, with a moderate hardness. Note that sp^3 content is not the only factor affecting the mechanical properties of the carbon film, since hardness values similar to ours have been reported for much higher sp^3 contents,[45,46] and very hard all-sp^2 structures can be also synthesized.[8] The hardness of fullerene-like films is mostly affected by the folding and crosslinking of basal planes. These fullerene-like structures are especially important in the case of graphitic carbon nitride films.[7,47]

V. CONCLUSIONS

The use of ion bombardment concurrent with carbon evaporation allows the synthesis of hydrogen-free carbon films with an sp^3 content of ~30%. The optimal ion assistance energy is in the range between 200 and 300 eV according to a subplantation mechanism. The use of more energetic ions increases the damage and resputtering of the film, producing a sharp reduction of the sp^3 content.

The sp^3 content affects macroscopic properties such as density and hardness. The density increases linearly with the sp^3 content. The hardness increases significantly, suggesting that the sp^3 content is not the only parameter affecting the mechanical performances. Folding of graphitic planes and crosslinking through sp^3 sites seem to be of major importance.

ACKNOWLEDGMENTS

This work has been partially financed by the Spanish CICYT under Project Nos. MAT96-0529 and PB97-1224, CAM Project No. AE 00140/94, NATO Project No. CRG-971539, and the US Department of Energy through Lawrence Livermore National Laboratory under Contract No. W-7405-ENG-48. The work was performed at the Stanford Synchrotron Radiation Laboratory, which is supported by the DOE, Office of Basic Energy Science. A grant from the F.P.U. program of the Spanish M.E.C. is also appreciated.

[1] J. Robertson, Curr. Opin. Solid State Mater. Sci. **1**, 557 (1996).
[2] J. C. Angus, F. Jansen, J. Vac. Sci. Technol. A **6**, 1778 (1988).
[3] J. Robertson, Adv. Phys. **35**, 317 (1986).
[4] J. Robertson, Pure Appl. Chem. **66**, 1789 (1994).
[5] H. W. Kroto, J. R. Heath, S. C. O'Brien, R. F. Curl, and R. E. Smalley, Nature (London) **318**, 162 (1985).
[6] S. Iijima, Nature (London) **354**, 56 (1991).
[7] H. Söjström, S. Stafström, M. Boman, and J. E. Sundgre, Phys. Rev. Lett. **75**, 1336 (1995).
[8] I. Alexandrou, H. J. Scheibe, C. J. Kiely, A. J. Papworth, G. A. J. Amaratunga, and B. Schultrich, Phys. Rev. B **60**, 10903 (1999).
[9] H. Hiura, T. W. Ebbesen, J. Fujita, K. Tanigaki, and T. Takada, Nature (London) **367**, 148 (1994).
[10] J. Robertson, Diamond Relat. Mater. **3**, 361 (1994).
[11] Y. Lifshitz, S. R. Kasi, and J. W. Rabalais, Phys. Rev. B **41**, 10468 (1990).
[12] R. Gago, O. Böhme, J. M. Albella, and E. Román, Diamond Relat. Mater. **8**, 1944 (1999).
[13] Y. Feng, Z. Zhou, Y. Zhou, and G. Zhou, Nucl. Instrum. Methods Phys. Res. B **86**, 225 (1994).
[14] J. A. Leavitt, L. C. McIntyre Jr., P. Stoss, J. G. Oder, M. D. Ashbaugh, B. Dezfouly-Arjomandy, Z. M. Yang, and Z. Lin, Nucl. Instrum. Methods Phys. Res. B **40/41**, 776 (1989).
[15] M. Mayer, *SIMNRA User's Guide* (Max-Plank-Institute für Plasmaphysik, 1997/98), v.4.0.
[16] M. M. Garcia, I. Jiménez, L. Vázquez, C. Gómez-Aleixandre, J. M. Albella, O. Sánchez, L. J. Terminello, and F. J. Himpsel, Appl. Phys. Lett. **72**, 2105 (1998).
[17] D. M. Gruen *et al.*, Appl. Phys. Lett. **68**, 1640 (1996).
[18] P. Bou and L. Vandenbulcke, J. Electrochem. Soc. **138**, 2991 (1991).
[19] M. A. Tamor and W. C. Vassell, J. Appl. Phys. **76**, 3823 (1994).
[20] W. C. Oliver and G. M. Pharr, J. Mater. Res. **7-6**, 1564 (1992).
[21] W. C. Oliver, R. Hutchings, and J. B. Pethica in ASTM Spec. Tech. Publ. **889**, 90 (1986).
[22] D. Lebouvier, P. Gilormini, and E. Felder, Thin Solid Films **172**, 227 (1979).
[23] F. Rossi *et al.*, J. Appl. Phys. **75**, 3121 (1994).
[24] W. T. Zheng, E. Broitman, N. Hellgren, K. Z. Xing, I. Ivanov, H. Sjöström, L. Hultman, and J. E. Sundgren, Thin Solid Films **308-9**, 243 (1997).
[25] R. Gago *et al.* (unpublished).
[26] J. Schwan, S. Ulrich, T. Theel, H. Roth, H. Ehrhardt, P. Becker, and S. R. P. Silva, J. Appl. Phys. **82**, 6024 (1997).
[27] I. Jiménez, D. G. J. Sutherland, J. A. Carlisle, A. van Buuren, L. J. Terminello, and F. J. Himpsel, Phys. Rev. B **57**, 13167 (1998).
[28] L. Fayette, B. Marcus, M. Mermoux, G. Tourillon, K. Laffon, P. Parent, and F. Le Normand, Phys. Rev. B **57**, 14123 (1998).
[29] J. Fink, T. Müller_Heizerling, J. Plüger, A. Bubenzer, P. Koidl, and G. Crecelius, Solid State Commun. **47**, 687 (1983).
[30] J. Kulik, G. D. Lempert, E. Grossman, D. Marton, J. W. Rabalais, and Y. Lifshitz, Phys. Rev. B **52**, 15812 (1995).
[31] J. Díaz, S. Anders, X. Zhou, E. J. Moler, S. A. Kellar, and Z. Hussain, J. Electron Spectrosc. Relat. Phenom. **103**, 545 (1999).
[32] I. Jiménez, M. M. García, J. M. Albella, and L. J. Terminello, Appl. Phys. Lett. **73**, 2911 (1998).
[33] D. Beeman, J. Silverman, R. Lynds, and M. R. Anderson, Phys. Rev. B **30**, 870 (1984).
[34] R. O. Dillon and J. A. Woollam, Phys. Rev. B **29**, 3482 (1984).
[35] H. J. Scheibe, D. Drescher, and P. Alers, Fresenius J. Anal. Chem. **353**, 695 (1995).
[36] F. Tuinstra and J. L. Koenig, J. Chem. Phys. **53**, 1126 (1970).
[37] D. C. McCulloch, S. Prawer, and A. Hoffman, Phys. Rev. B **50**, 5905 (1994).
[38] M. Yoshikawa, G. Katagari, H. Ishida, A. Ishitani, and T. Akamatsu, J. Appl. Phys. **64**, 6464 (1988).
[39] P. J. Fallon, V. S. Veerasamy, C. A. Davis, J. Robertson, G. A. J. Amaratunga, W. I. Milne, and J. Koskinen, Phys. Rev. B **48**, 4777 (1993).
[40] J. Schwan, S. Ulrich, H. Roth, H. Ehrhardt, S. R. P. Silva, J. Robertson, R. Samlenski, and R. Brenn, J. Appl. Phys. **79**, 1416 (1996).
[41] B. André, F. Rossi, A. van Veen, P. E. Mijnareds, H. Schut, and M. P. Delplancke, Thin Solid Films **241**, 171 (1994).
[42] E. Grossman, G. D. Lempert, J. Kulik, D. Marton, J. W. Rabalais, and Y. Lifshitz, Appl. Phys. Lett. **68**, 1214 (1996).
[43] R. Gago, O. Sánchez-Garrido, A. Climent-Font, J. M. Albella, E. Román, J. Räisänen, and E. Raühala, Thin Solid Films **338**, 88 (1999).
[44] D. R. McKenzie, D. Muller, and B. A. Pailthorpe, Phys. Rev. Lett. **67**, 773 (1991).
[45] S. Logothetidis and C. Charitidis, Thin Solid Films **353**, 208 (1999).
[46] N. Savvides and T. J. Bell, Thin Solid Films **228**, 289 (1993).
[47] N. Hellgren, M. P. Johansson, E. Broitman, L. Hultman, and J. Sundgren, Phys. Rev. B **59**, 5162 (1999).